Ultrasound in Med. & Biol., Vol. 29, No. 4, pp. 517–528, 2003

0301-5629/03/$–see front matter

ELSEVIER

doi:10.1016/S0301-5629(02)00704-4

● *Original Contribution*

IMPLEMENTATION ISSUES IN ULTRASONIC FLOW IMAGING

S. KAISAR ALAM* and KEVIN J. PARKER†
*Riverside Research Institute, New York, NY, USA; and †Center for Biomedical Ultrasound and Electrical and Computer Engineering, University of Rochester, Rochester, NY, USA

(*Received* 28 *May* 2002; *in final form* 17 *September* 2002)

Abstract—This article addresses several implementation issues in ultrasonic flow imaging. We discuss frequency-dependent scattering and attenuation, use of interpolation for computation intensive methods and implications of the use of chirps to increase bandwidth. We also discuss wall filtering issues; our observations show that the butterfly search estimator may be capable of *detecting* flow in the vicinity of strong stationary scatterers (clutter) without additional processing such as wall-filtering. Illustrative examples are given for simulated and experimental data. (e-mail: parker@ece.rochester.edu) © 2003 World Federation for Ultrasound in Medicine & Biology.

Key Words: **Blood flow, Color Doppler imaging, Color flow imaging, Doppler ultrasound, Flow, Pulsed Doppler, Tissue motion, Ultrasound, Ultrasonic imaging, Ultrasonography, Wall filters.**

INTRODUCTION

Background

Real-time ultrasonic flow imaging plays a major role in the diagnosis of many diseases, especially cardiac diseases. Recently, it also has been found useful in identifying cancers, such as those of the breast (ATL 1994). Real-time ultrasonic flow imaging became feasible after the development of the autocorrelation estimator by Kasai et al. (1985). Since then, investigators described many alternative approaches; these include Alam and Parker (1995), Bonnefous and Pesque (1986), Ferrara and Algazi (1991a; 1991b), Foster et al. (1990), Loupas et al. (1995), Torp and Kristoffersen (1995), and Vaitkus and Cobbold (1998). However, many modern commercial machines use the autocorrelation method, primarily due to its computational simplicity and the high computational complexity of the alternative methods. However, with the recent advances in processing speed, real-time implementation of complex algorithms may become feasible. Ferrara and DeAngelis (1997) review color flow imaging.

In this article, we address several implementation issues of flow imaging. We will discuss these issues in reference to the butterfly search; however, much of the discussion is equally applicable to other flow-imaging methods. The butterfly search was introduced by Alam and Parker (1995). Alam (1996) has demonstrated, using various performance measures with simulated and experimental data, that the performance of the butterfly search is significantly superior to that of conventional methods under noisy conditions and in the presence of substantial signal decorrelation. The butterfly search method was derived to track the axial movement of a group of scatterers between transducer bursts. (Alam (1996) discussed the feasibility of extending the butterfly search for angle-independent flow measurement.) When a scatterer moves, it affects both the phase and time delay of RF echoes. Most ultrasonic tissue-motion estimation methods analyze either delay or phase change. The butterfly search method makes use of the fact that a specific rate of scatterer movement is associated with a unique combination of phase- and time-delay over repeated transducer bursts. A search is made to identify the trajectory where this combination is satisfied.

Flow estimation methods can be grouped into three principal categories, primarily based on the signal models: 1. the frequency/phase (Doppler) methods, 2. the time-domain methods, and 3. the multiple-burst (tracking) methods. The methods are sometimes classified into narrowband and wideband methods.

The frequency/phase (Doppler) methods. If ultrasound (US) echo is sampled at a fixed depth over repeated transducer bursts, there will be a change of phase

Address correspondence to: K. J. Parker, University of Rochester, Rochester NY 14627 USA. E-mail: parker@ece.rochester.edu

in the returned echo from the sample volume in the presence of flow. The rate of change of phase (or the frequency) is proportional to the tissue velocity. However, aliasing occurs if tissue moves more than a quarter of the wavelength between transducer bursts. The breakthrough implementation for color flow imaging came from this group of estimators (Kasai et al. 1985). The velocity is computed from the phase of the autocorrelation of sampled complex envelopes at unity lag. The frequency-domain methods use relatively narrowband pulses and, typically, use eight or more transducer bursts. Magnin (1986) is an excellent tutorial paper on Doppler US, and Burns (1987) and Magnin (1987) contain excellent overviews of the conventional Doppler methods. Jensen (1996) and Jones (1993) also contain comprehensive overviews on the estimation of blood velocity with US. For comprehensive analysis of Doppler US systems, readers can see Azimi and Kak (1985). Kremkau (1990); (1991) and Wells (1994) provide excellent summaries of color flow applications.

The time-domain methods. The relative time shift in echoes due to target movement between two successive firings can also be used to estimate flow. Different groups independently implemented a cross-correlation search to estimate this shift (Bonnefous and Pesque 1986; Foster et al. 1990). Because the correlation search is computationally intensive, a 1-bit version has been commercially implemented for real-time operation (Bonnefous et al. 1986; Rickey et al. 1992). To reduce the computational complexity for the correlation search, a sum-absolute-difference (SAD) algorithm has been proposed (Bohs and Trahey 1991). Time-domain search methods generally use wideband pulses and do not suffer from aliasing. de Jong et al. (1990) developed a narrowband method that calculates the correlation coefficient function only at five points in the vicinity of the maximum, and uses an interpolation algorithm to evaluate the location of correlation maximum from these points. This method requires significantly less computation than correlation search; however, it does not work well with large band width signals, and suffers from aliasing. A comprehensive review of the time-domain methods can be found in Hein and O'Brien (1993).

Multiple-burst (tracking) methods. These methods are based on both the phase change and the relative time shift in the echoes. Frequency/phase-domain methods use the change of phase over many transducer bursts from only a fixed sample volume, whereas time-domain methods, at least in the simplest implementation, try to estimate the tissue movement through the time shift between two successive transducer bursts. However, the new tracking methods try to track the target movement using various algorithms through many transducer bursts. In this model, the radiofreequency (RF) echoes due to many transducer bursts are stacked together to form a 2-D array ("slow time"–transducer burst index, "fast time"–depth). The 2-D array thus created may be processed in a variety of ways to obtain a flow estimate. These are generally wideband methods, but some suffer from aliasing artefact.

Wilson (1991) has shown that 2-D Fourier transform of 2-D RF array is nonzero only along radial line segments on the frequency plane where the slope is proportional to the scatterer velocity. A method to overcome the associated frequency aliasing problem was also discussed. Loupas and Gill (1994) analyzed the problem of 2-D spectral analysis for discrete limited-duration signals. Loupas et al. (1995) introduced a 2-D autocorrelation approach for the axial velocity estimation. This approach estimates both the center frequency and the mean Doppler frequency and, thus, can potentially overcome the estimator bias due to frequency-dependent attenuation discussed in Ferrara et al. (1992). The results from simulation showed that 2-D autocorrelation performs much better in the presence of modest velocity spread and high signal-to-noise ratio (SNR); however, these enhancements become marginal as the condition worsens, reducing the correlation between Doppler and RF fluctuations.

Ferrara and Algazi (1991a) developed a sophisticated matched filter approach to flow estimation, referred to as the wideband maximum likelihood estimator (WMLE). This approach uses an *a priori* complex envelope signal model from a slowly fluctuating point target model for the matched filter. Torp and Kristoffersen (1995) presented a tracking method that suppresses frequency aliasing in the Doppler spectrum velocity-time display. They demonstrated that tracking in 2-D transform space, as described by Wilson (1991), can be shown to be equivalent to a tracking in 2-D (slow time–fast time) space.

Alam and Parker (1995) developed the "butterfly search" for envelope, RF or complex envelope signals from a deterministic analysis (the latter derived using Schwartz's inequality), based on the common signal model used in all methods in this group. In the latter method, the complex envelope is sampled on different delay trajectories (butterfly lines) on slow time–fast time space. Each butterfly line, representing a unique (constant) flow velocity, is associated with a unique frequency. The butterfly sampled complex envelope is examined for the power at the frequency corresponding to that butterfly line, normalized by the total power. On each butterfly line, the ratio shown in eqn (5) is evaluated. Two techniques were later introduced to reduce the computational complexity of the method and provide

simpler hardware implementation (Alam and Parker 1996). A detailed analysis and comparison with the conventional methods are presented in Alam (1996).

Under a number of specific assumptions and key modifications, the WMLE could be modified into the form of the butterfly search on quadrature components (Alam and Parker 1995). Discrete radon transform, which has uses in beamforming (Johnson and Dudgeon 1993), could also be related logically to the butterfly search. See Durrani and Bisset (1984) for an overview of radon transform and its properties.

Tracking methods have been found to perform well. Some of these methods suffer from notable limitations, including aliasing effects in the 2-D Fourier fast transform and the necessity to accurately know the received signal shape in the WMLE. These methods are, typically, computation-intensive; however, with the recent advances in processing speeds, this may not be a significant limitation.

Butterfly search

A simplified 1-D model was used in Alam and Parker (1995) to derive the butterfly search estimator. For a point target moving toward the transducer, if the velocity v_0 is constant, then the nth RF A-line can be shown to have the following form:

$$s(n, t) = A\cos\left\{\omega_0\left[t - 2\frac{d}{c} + 2n\frac{\nu_0}{c}T\right]\right\} \times r\left\{t - 2\frac{d}{c} + 2n\frac{\nu_0}{c}T\right\}, n = 0,1,2,\cdots,N-1, \quad (1)$$

where A is the signal amplitude, n is the index for the repeated transducer bursts, T is the pulse-repetition period, d is the distance of the object from the transducer at the first transducer burst ($n = 0$), ω_0 is the angular center frequency, c is the sound propagation speed, and $r(\ )$ is the envelope of the transmitted pulse (frequently modeled as Gaussian, maximizing at $t = 0$). The factor of 2 in the expression comes from the round-trip travel of the wave. Time-axis origin is reset at each transducer burst. System effects are neglected.

For the RF signal in eqn (1), the complex envelope can be expressed as:

$$\tilde{r}(n, t) = \tilde{A}\exp - j\left[2\omega_0 n\frac{\nu_0}{c}T\right] r\left\{t - 2\frac{d}{c} + 2n\frac{\nu_0}{c}T\right\}, \quad (2)$$

where

$$\tilde{A} = \frac{A}{2}\exp j\left[2\omega_0\frac{d}{c}\right]. \quad (3)$$

This signal can be resampled at depth d along trajectories describing lines of constant velocity in (n, t) space. If $\tilde{r}_{B\nu}[n]$ denotes the resampling of the complex envelope along the line for velocity v:

$$\tilde{r}_{B\nu}[n] = \tilde{r}(n, t)\big|_{t=2\frac{d}{c}-2n\frac{\nu}{c}T} = \tilde{A}\exp - j\left[2\omega_0 n\frac{\nu_0}{c}T\right] r\left\{2n\frac{\nu_0 - \nu}{c}T\right\}. \quad (4)$$

When $\nu = \nu_0$, $\tilde{r}_{B\nu_0}[n] = \tilde{A}\exp - j[2\omega_0 n(\nu_0/c)T]r(0)$. Thus, in the absence of noise, on the correct butterfly line for a single point target, complex envelope samples along the butterfly line corresponding to correct flow velocity would be a single-frequency complex exponential. Each flow velocity corresponds to a unique frequency. If we examine each butterfly line for the power at the frequency corresponding to that butterfly line, normalized by the total power, the maximum should occur on the correct line ($\nu = \nu_0$). On an incorrect line, the butterfly-sampled complex envelope is given by eqn (4) for $\nu \neq \nu_0$. Here, the spectrum of $\tilde{r}_{B\nu}[n]$ would have the maximum at $\omega = -2\omega_0(\nu_0/c)T$, and not at $\omega = -2\omega_0(\nu/c)T$ (the frequency corresponding to that butterfly line); the energy would be spread according to the spectrum of the envelope term $r(\ )$.

The following ratio is computed for a range of target velocities, ν,

$$L(\nu) = \frac{\left|\sum_{n=0}^{N-1}\tilde{r}_{B\nu}[n]e^{j2\omega_0 n\frac{\nu}{c}T}\right|^2}{\sum_{n=0}^{N-1}|\tilde{r}_{B\nu}[n]|^2} \quad (5)$$

Each ν denotes a butterfly line and $L(\nu)$ maximizes at the correct target velocity. (Expression for $L(\nu)$ can also be normalized by N, so that $L \leq 1$.) A search is conducted for a velocity ν that maximizes $L(\nu)$. This method is especially adept at accurate flow estimation in the presence of substantial noise and decorrelation because it uses the combination of delay and phase change instead of only one of them. The robustness of the butterfly search technique has been independently verified by researchers in other laboratories (Vogt and Ermert 1997).

Models and experiment

Results reported in this paper were produced using data generated from simulation and experiments. The initial evaluation of the butterfly search technique was performed using data generated from a 1-D simulation model. Later simulations were performed using a detailed 3-D model, based on point scattering; contributions from the moving scatterers were summed to get an

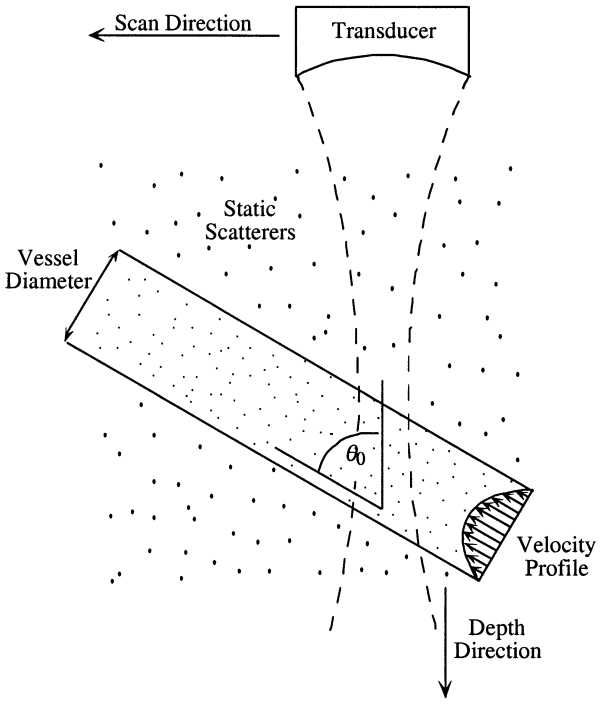

Fig. 1. 3-D scattering volume model. Out of plane is the azimuthal direction.

RF A-line. Because of the relatively long wavelength of 5-MHz pulses, the point scatterer model is a good approximation; it would be less accurate at higher (*e.g.*, > 50 MHz) transducer frequencies (Hunt et al. 1995). Figure 1 shows the cross-sectional view of the 3-D scattering volume of simulation geometry. A cylindrical vessel, carrying the moving scatterers, is embedded in the tissue comprised strong stationary scatterers (clutter). The vessel axis lies on the image plane and is at an angle θ_0 with the direction of propagation; thus, lateral movement of the scatterers will produce some speckle decorrelation. The effects of US beam geometry (*e.g.*, focusing, sidelobes, grating lobes) and the frequency-dependent attenuation of the intervening tissue were ignored. The beam is Gaussian in both lateral and azimuthal directions. In short, the simulation consists of 3-D random scatterers convolved with a nondiffracting 3-D acoustic pulse (1-mm beam width). The velocity profile is parabolic ($v = V_{max}[1 - (r/R)^2]$). In the simulation we used, r = 0.5 cm, $\theta_0 = 45°$ and $V_{max} = 100$ cm/s. For the simulated 2-way pulse, $f_0 = 4$ MHZ, bandwidth = 56% (−6 dB). Number of A-lines = 3, and SNR = 3 dB. (Maximum velocity in the direction of propagation was 70.71 cm/s.) The ratio of stationary clutter to moving scatterer strength was 40 dB (*i.e.*, the moving "blood" is hypoechoic). RF echo signals were sampled at 40×10^6 cycles/s. No vessel wall was simulated. The velocity of each scatterer was assumed unchanged through the scanning process. A scatterer concentration of 64 mm^{-3} was used. The initial 1-D simulation model used a similar two-way acoustic pulse (5-MHz center frequency and 56% fractional bandwidth), unless indicated otherwise; a total of 67 scatterers/mm were simulated, which was more than sufficient for fully developed speckle. $f_s = 50 \times 10^6$ cycles/s.

Flow-phantom experimental data used in this paper were acquired by Embree and Mayo (1987). The same data set had been widely used to evaluate flow estimator performance (Alam 1996; Ferrara and Algazi 1991b; Vaitkus 1995). The setup used Sephadex G-10 particles traveling in a 50% glycerin-water solution through a straight dialysis tube of 7-mm diameter. The hydrodynamic flow rate was 281 mL/min; using parabolic flow profile assumption, the peak velocity was 24.3 cm/s and the axial component of this velocity was 17.2 cm/s. Flow direction was at a 45° angle with the beam. The transducer focal point was located at the midpoint of the vessel, where the −3 dB beam width was 0.8 mm. The transducer center frequency was 5 MHz with a band width (−3 dB, one-way) of 2.5 MHz. The amplified RF echo was sampled at 50 MHz and immediately digitized using 8 bits. A total of 384 A-lines were acquired at a pulse-repetition frequency (PRF) of 7812.5 Hz. Each A-line had 1024 samples. We have also acquired experimental data using flow-phantoms; results and details about data-acquisition are described in detail in Alam (1996). This article addresses methods and results in Alam (1996) that have not been published elsewhere.

IMPLEMENTATION ISSUES

Frequency-dependent scattering and attenuation

Distortion of the echo from blood by the intervening media can affect blood velocity estimation. The effect of frequency-dependent scattering and attenuation can be expressed in terms of a shift in the center frequency in the resulting echo, and virtually all methods that use a complex envelope for flow estimation are susceptible to a scale factor bias (Ferrara et al. 1992). We have shown (Alam 1996) that, for a downshift in the center frequency from ω_0 to $\omega_0 - \Delta\omega$, velocity estimated by the butterfly search would be scaled by a factor $(\omega_0 - \Delta\omega)/\omega_0$ (underestimation). However, if there is *a priori* knowledge about frequency-dependent scattering and attenuation, the downshift in the center frequency could be included in the evaluation of $L(v)$. Ferrara et al. (1992) suggested using this *a priori* knowledge for velocity estimation using WMLE. However, such information might not always be available. The cross-correlation search technique requires no such compensation procedure in the presence of frequency-dependent scattering and attenua-

tion, because it compares successive echoes, both of which would go through the same distortion. However, our results show that cross-correlation is not as robust as the butterfly search in the presence of noise and decorrelation.

Interpolation of L(ν)

In many flow estimation methods, flow velocity is estimated by determining a maximum; in the butterfly search, the maximum of $L(\nu)$ is estimated. This maximum can be found using brute force methods that use very small increments of ν. However, this is not practical due to computational inefficiency. For real-time flow estimation, efficient estimation of the peak of $L(\nu)$ is necessary. Parabolic interpolation could be used to locate the peak of $L(\nu)$; a similar approach has been used to locate the peak of cross-correlation functions (Foster et al. 1990).

A function has to be continuous in the region-of-interest (ROI) for peak interpolation. The primary peak of $L(\nu)$ has approximately a $|\text{sinc}(\ )|$ form and the width of the primary peak of $L(\nu)$ is inversely related to center frequency and number of A-lines (Alam 1996). (The $|\text{sinc}(\ )|$ behavior is apparent in Fig. 3a around the main lobe.) When the widths of the main lobe and side lobes become large, this effect cannot be seen. Because $L(\nu)$ is a well-behaved function, at least within the main lobe, the peak of $L(\nu)$ may be estimated by interpolating between the sampled peak of $L(\nu)$ and its two nearest neighbors. Figure 2a illustrates this concept using a 1-D simulation. Figure 2b shows the same graph expanded around the peak. The interpolated peak (using a parabolic interpolation function) and the true peak are very close to each other. The bias is -0.311 cm/s. If we chose to space the butterfly lines half samples apart, then the bias would be -0.048 cm/s and at two sample delay, it would be -0.9456 cm/s.

For valid interpolation, all three samples of $L(\nu)$ used in the interpolation need to be on the primary peak. If they are too far apart, then the primary peak can be completely missed. We have derived the rule of thumb that the separation between the $L(\nu)$ samples should not exceed -3 dB width of the primary peak. For the case shown in Fig. 3, the -3 dB width of the peak corresponds to an approximately three-sample shift between transducer bursts. Although a three-sample shift is adequate for not missing a peak, error in estimating the peak using interpolation increases when sampling interval increases (Alam and Ophir 2000; Céspedes et al. 1995). So, we typically use a unity sample shift between consecutive butterfly lines. Although it is desirable to have a sharp $L(\nu)$ peak, if the peak is very sharp, the possibility of missing the primary peak or not having all the sample points on the primary peak increases. It is rather advantageous that peak interpolation works very well when butterfly lines lie on sample points with typical processing and ultrasonic imaging parameters.

Pulse compression methods

Pulse compression techniques for ultrasonic imaging by transmitting chirp signals, instead of the conventional pulse, has been proposed by Rao et al. (1988). This allows the peak intensity of the transmitted pulse to be low without loss of axial resolution (or, in other words, the bandwidth can be wide.)

For a system using chirps, the transmitted pulse has the form, $p(t) = A\cos(\omega_0 t + \Delta_\omega t^2/2)r(t)$. The instantaneous radial frequency of this pulse is given by $\omega(t) = \omega_0 + \Delta_\omega t$. For a pulse interval of $(-T_p/2, T_p/2)$, the frequency (radial) sweep is from $\omega_0 - \Delta_\omega T_p/2$ to $\omega_0 + \Delta_\omega T_p/2$.

Then, the complex envelope can be shown to be:

$$\tilde{r}(n, t) = A \exp j\left\{2\omega_0\left[\frac{d}{c} - n\frac{\nu_0}{c}T\right] + \frac{\Delta\omega}{2}\left[t - 2\frac{d}{c} + 2n\frac{\nu_0}{c}T\right]^2\right\} \times r\left\{t - 2\frac{d}{c} + 2n\frac{\nu_0}{c}T\right\}, \quad n = 0,1,2, \cdots, N-1. \quad (6)$$

Then, on a butterfly line,

$$t - 2\frac{d}{c} + 2n\frac{\nu}{c}T = 0, \quad (7)$$

the butterfly sampled complex envelope:

$$\tilde{r}_{B\nu}[n] = \tilde{r}(n, t)\big|_{t=2\frac{d}{c}-2n\frac{\nu}{c}T} = A \exp j\left\{2\omega_0\left[\frac{d}{c} - n\frac{\nu_0}{c}T\right] + \frac{\Delta\omega}{2}\left[2n\frac{\nu_0 - \nu}{c}T\right]^2\right\} r\left\{2n\frac{\nu_0 - \nu}{c}T\right\}. \quad (8)$$

Quite clearly, on any butterfly line other than $\nu = \nu_0$, the sampled complex envelope will not even be composed of simple sinusoids because of the quadratic phase term. However, on the correct butterfly line, the sampled complex envelope will be a constant amplitude and single-frequency complex exponential, as shown below. Thus, the butterfly search can be used unmodified with chirp transmission. (Correlation-based methods can be used unmodified, as well.)

$$\tilde{r}_{B\nu_0}[n] = A \exp j\left\{2\omega_0\left[\frac{d}{c} - n\frac{\nu_0}{c}T\right]\right\} r\{0\}. \quad (9)$$

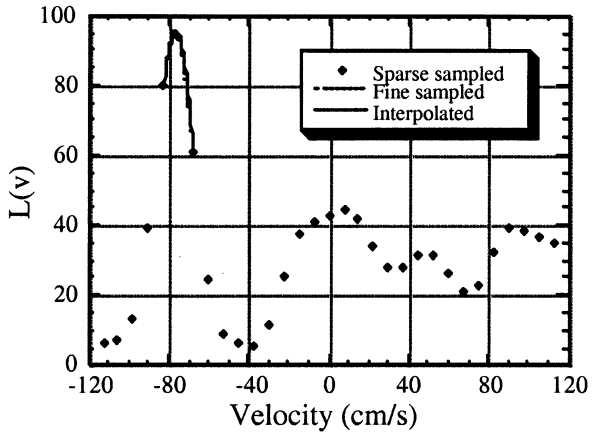

(a)

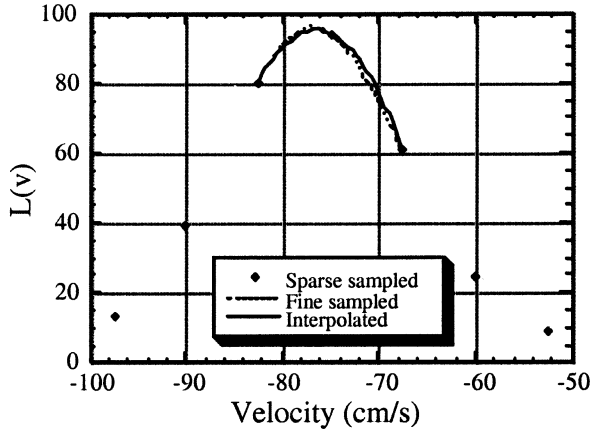

(b)

Fig. 2. (a) Interpolation of $L(\nu)$. Number of lines = 3. (b) More details than (a) shown around the peak.

In Fig. 3, results from 1-D simulation are shown to demonstrate the effect of bandwidth and chirps instead of regular pulses. Only Fig. 3f has additive noise (SNR = 0 dB). At a lower σ (pulse envelope: $r(t) = e^{-2(\pi\sigma t)^2}$), the subsidiary peaks of $L(\nu)$ are comparable to the primary peak. On the other hand, use of chirps produces lower subsidiary peaks at low σ. However, at higher σ, perhaps because the bandwidth is high to begin with, improvements are minimal. When the number of A-lines is increased, the primary peak becomes sharper; however, it does not noticeably affect the height of the subsidiary peaks. With the addition of noise, the base level of $L(\nu)$ increases. Thus, the butterfly search can be directly applied to the reflected echoes for chirp transmission. And, because the butterfly search is a broadband method, it can also be applied after pulse compression processing.

Wall filtering

Suppression of "clutter" is a major issue in color flow imaging. Clutter refers to the strong echo signal from the stationary or slowly moving wall and tissues close to vessel walls. Even when the sample volume is farther away from the vessel walls than the width of the system impulse response, clutter might still be present due to the 3-D nature of sample volume, sidelobes, refraction, multiple reflections, range ambiguity, etc. Unless adequately suppressed, clutter will dominate the weak echo from blood, suppressing the velocity information. Ineffective clutter suppression results in residual Doppler signal power leading to poor overall flow visualization. Common wall filters to remove clutter had been discussed by Willemetz et al. (1989). The simplest wall filter is the single echo-canceller (first difference filter),

$$H_1(z) = (1 - z^{-1}). \tag{10}$$

However, this filter is not appropriate for slow flow estimation due to poor low frequency response. Moreover, this filter reduces the SNR (Jansen 1991). The frequency response can be improved by cascading two such filters (double echo-canceller),

$$H_2(z) = (1 - 2z^{-1} + z^{-2}). \tag{11}$$

These are finite impulse response (FIR) type filters (no feedback). The frequency response can be greatly improved by adding feedback, thereby converting them to infinite impulse response type (IIR). The first-order and the second-order IIR filters have the forms:

$$H_1(z) = \frac{1 - z^{-1}}{1 - Kz^{-1}}, \tag{12}$$

$$H_2(z) = \frac{1 - 2z^{-1} + z^{-2}}{1 + K_1 z^{-1} + K_2 z^{-2}}. \tag{13}$$

Wall filters can introduce bias and an effect similar to aliasing in the presence of noise (Willemetz et al. 1989; Nowicki et al. 1990). Willemetz et al. (1989), Tysoe and Evans (1995), and Rajaonah et al. (1994) discussed how to compensate for them. IIR filters perform better in this respect. Brands et al. (1995) introduced an adaptive wall filter that adapts its rejection range to the temporal mean frequency of the clutter. Suorsa et al. (1990) discussed the role of wall filtering in the context of correlation-based flow measurement. Performance of IIR filters depends on their transient responses that, in turn, depends on the initialization scheme (Kadi and Loupas 1995). Success of a given initialization strategy depends on how

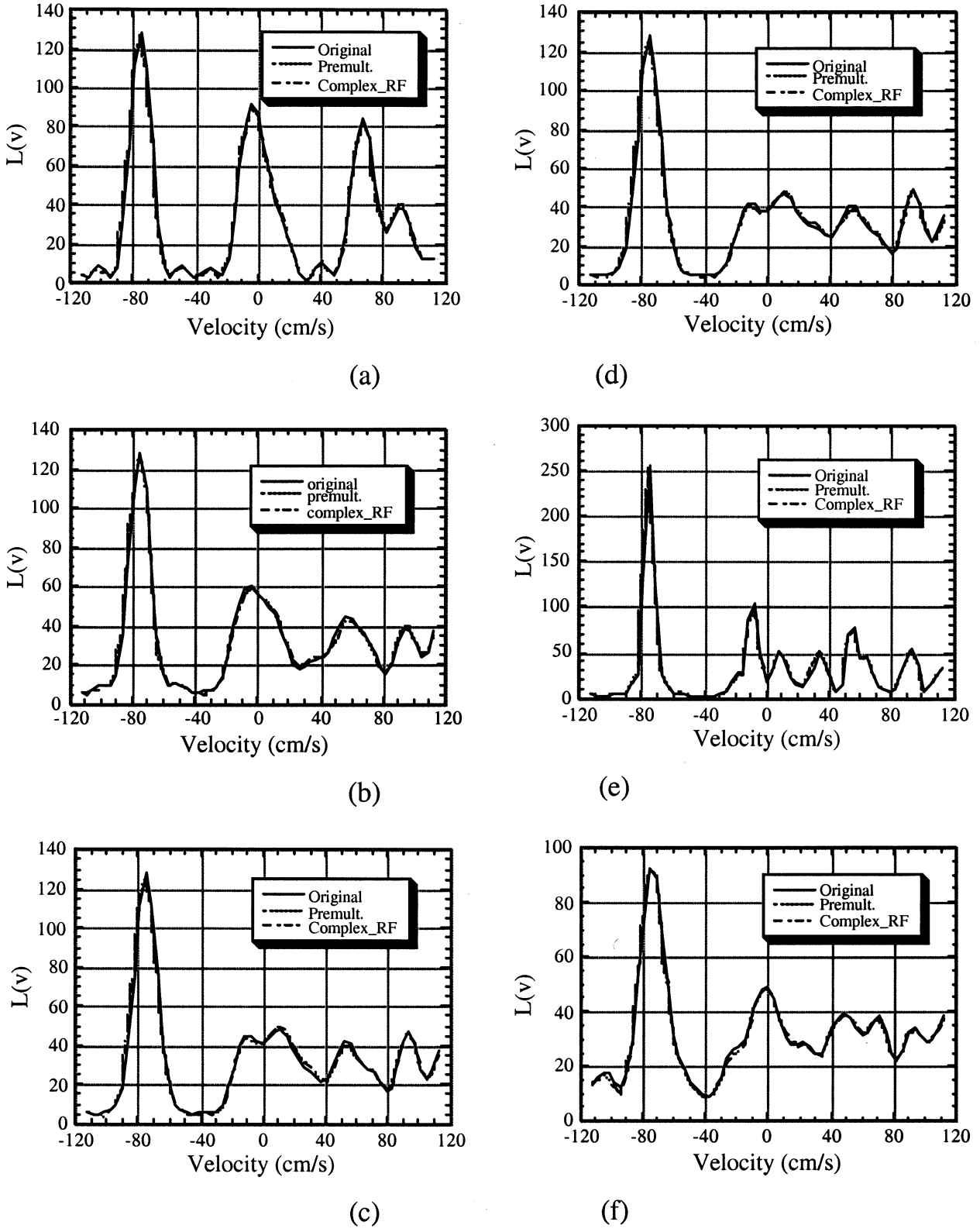

Fig. 3. (a) $L(\nu)$ for a narrowband pulse (σ = 0.41 MHz). Number of lines = 4. (b) Chirp (σ = 0.41 MHz, Δf = 1.34 MHz/μs). Number of lines = 4. (c) Wideband pulse (σ = 1.41 MHz). Lines = 4. (d) Chirp (σ = 1.41 MHz, Δf = 3.33 MHz/μs). Lines = 4. (e) Wideband pulse (σ = 1.41 MHz). Lines = 8. (f) Wideband pulse (σ = 1.41 MHz). Lines = 4, SNR = 0 dB.

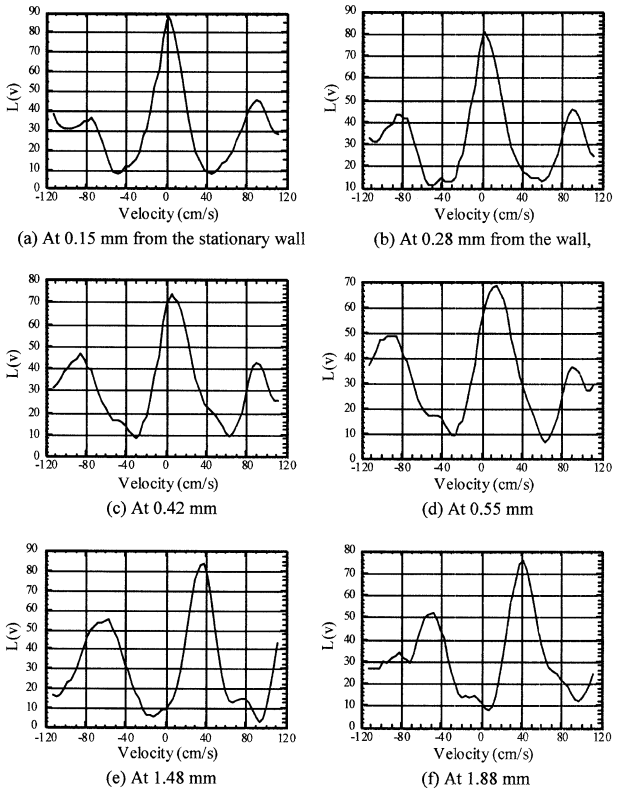

Fig. 4. Illustration of behavior of $L(\nu)$ close to the wall surface. The butterfly search method can show flow even in the presence of strong stationary clutter. (See Table 1 for more details.)

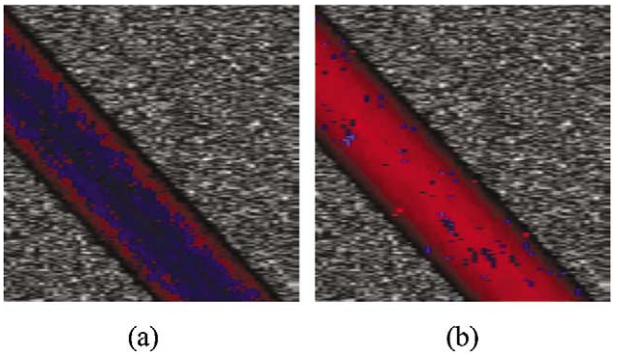

Fig. 5. Duplex images showing blood vessel embedded in tissue (3-D simulation). V_{max} (axial) = 66.67 cm/s, θ = 45°, Clutter-to-blood ratio = 40 dB, SNR = 3 dB, and number of RF lines = 3. (a) Autocorrelation method; (b) butterfly search method; it is significantly cleaner and does not suffer from aliasing.

well it approximates the clutter component. A few articles discussed step-initialized IIR filters (Shariati et al. 1993), evaluation of IIR initialization schemes (Peterson et al. 1994), and adapting wall filtering to the mean frequency of the tissue component (Thomas and Hall 1994). Kadi and Loupas (1995) compared the performances of regression filters and IIR filters; wall filter performance generally depends heavily on the clutter-to-signal ratio and improves significantly when the number of A-lines is increased.

We have investigated wall filtering in the context of the butterfly search. We have discovered that the butterfly search technique can *detect* the flow of hypoechoic blood without wall filtering in the proximity of vessel walls. First, we will show the effect of clutter on $L(\nu)$. Then, we will show that butterfly search can detect flow close to vessel walls in large vessels. We will also show, using color flow images, that the butterfly search can detect blood flow in small vessels without wall filtering.

Figure 4a–g plots $L(\nu)$ vs. ν for increasing distance from the vessel wall for the 3-D model shown in Fig. 1. For the A-line used, the vessel boundaries were at 7 mm and 21 mm. As shown in Table 1, for the commonly implemented autocorrelation method, velocity estimates are near zero until the echo amplitude from blood is comparable to that of tissue. On the contrary, the butterfly search detects flow close to vessel walls (Fig. 4b–f) although the trailing edge of stationary tissue echo dominates blood echo. Off course, butterfly search underestimates the velocity when clutter is much stronger than blood. However, underestimation is minimal in this example when this ratio is less than 18 dB. (The results are summarized in Table 1. Estimated flow profiles are shown in Fig. 7.) We postulate that $L(\nu)$ does not significantly depend on signal amplitude due to the normalizing factor in $L(\nu)$, see eqn (5). Because the flow velocity

Table 1. Estimated flow velocities close to the vessel wall

Case	Distance from wall (mm)	Echo level larger than blood (dB)	True velocity (cm/s)	Butterfly search (cm/s)	Autocorrelation (cm/s)
(a)	0.15	35.6	4.2152	1.88	0.39
(b)	0.28	33.0	7.7926	2.34	0.27
(c)	0.42	31.5	11.2894	6.33	0.12
(d)	0.55	17.9	14.6684	13.36	−0.14
(e)	1.48	3.6	35.6085	35.86	32.65
(f)	1.88	0	43.0812	40.08	41.43

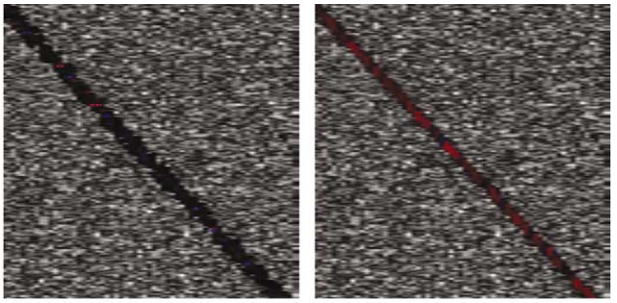

(a) (b)

Fig. 6. Duplex images for plug flow in a small vessel. No wall filtering was used. V_{max} (axial) = 6.67 cm/s, θ = 45°, Clutter-to-blood ratio = 40 dB, SNR = 3 dB, and number of RF lines = 3. (a) Autocorrelation method; (b) butterfly search method; it can detect blood flow pretty well inside the vessel.

close to the wall is slow, primary peak of $L(\nu)$, which depends on the combined effect of slow-moving blood and stationary tissue, will show presence of flow. However, as shown in Table 1, interaction of the contribution from tissue and blood will bias these flow estimates (toward smaller values), which should be investigated further in the future.

Figure 5 shows the duplex (color Doppler superimposed on B-mode) images for the same 3-D model for the butterfly search and autocorrelation technique. We have used standard red and blue color codes for all flow images. The autocorrelation technique suffers from aliasing and large estimation errors. The butterfly search duplex image clearly depicts the parabolic flow profile. These images also show that the butterfly search detects flow close to the wall, whereas the autocorrelation method does not.

Figure 6 further exhibits the ability of the butterfly search technique in detecting blood flow in small vessels without wall filtering. A 1-mm vessel was simulated carrying plug flow (7.07 cm/s in the beam direction). Other parameters were the same as the prior simulation. The autocorrelation technique failed to show blood flow in the vessel. On the other hand, the red color within the vessel depicts the blood flow in the vessel when the butterfly search was used. Clearly, contribution from clutter has introduced bias in the peak of $L(\nu)$; estimated velocities were $\approx$1 cm/s inside the vessel. However, detection of flow is frequently enough for diagnosis and, in such cases, the bias is not a significant issue. The decreased need for a wall filter is a practical and computational advantage.

ESTIMATOR PERFORMANCE

One-dimensional plots of results in Fig. 5 are shown in Fig. 7a. This plot also includes results for the two simplified butterfly methods introduced in Alam and Parker (1996). For all the three butterfly search methods, the parabolic profile of the flow is nicely reproduced even at low SNR environment. In comparison, the autocorrelation method shows aliasing. Despite the spatial averaging to reduce the effect of noise, it also shows large errors. We can clearly see that the autocorrelation technique failed to detect the flow close to the wall (strong echo), whereas, the quadrature butterfly search did not. Fig. 7b demonstrates the performance of the $L(\nu)$ interpolation. This interpolation works nearly as well as the brute force butterfly method, also in the vicinity of the wall. As expected, errors seem to increase with increase in $L(\nu)$ sample spacing.

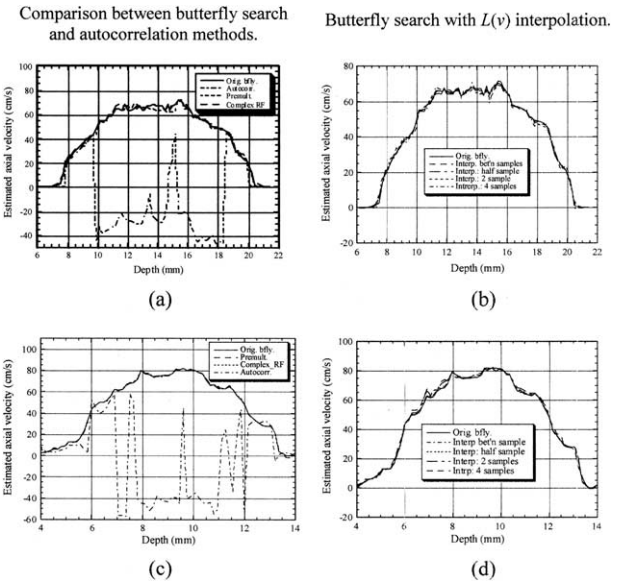

Fig. 7. Estimated flow profiles. (a)–(b) 3-D model; (c)–(d) Embree flow phantom data. Number of RF A-lines = 3.

The estimation results for the flow phantom data by Embree and Mayo (1987) are shown in Fig. 7c. The number of RF lines = 3 and SNR = 5 dB. (SNR for the original data were 20 dB. We added appropriate white noise to reduce SNR.) We used every fifth RF line for the velocity estimation; resulting in an effective peak axial midstream velocity of 85.9 cm/s. The performances of different techniques are very similar to those in Fig. 7a. Fig. 7d demonstrates the performance of the $L(\nu)$ interpolation applied on this data, which, again, performs quite well.

We also estimated the velocity profiles for the same data set using different methods for all 384 A-lines for a better understanding of the performances of the butterfly search and the conventional techniques in real flow conditions. Then the mean and the standard deviation (SD) of the velocity estimates vs. depth were computed and

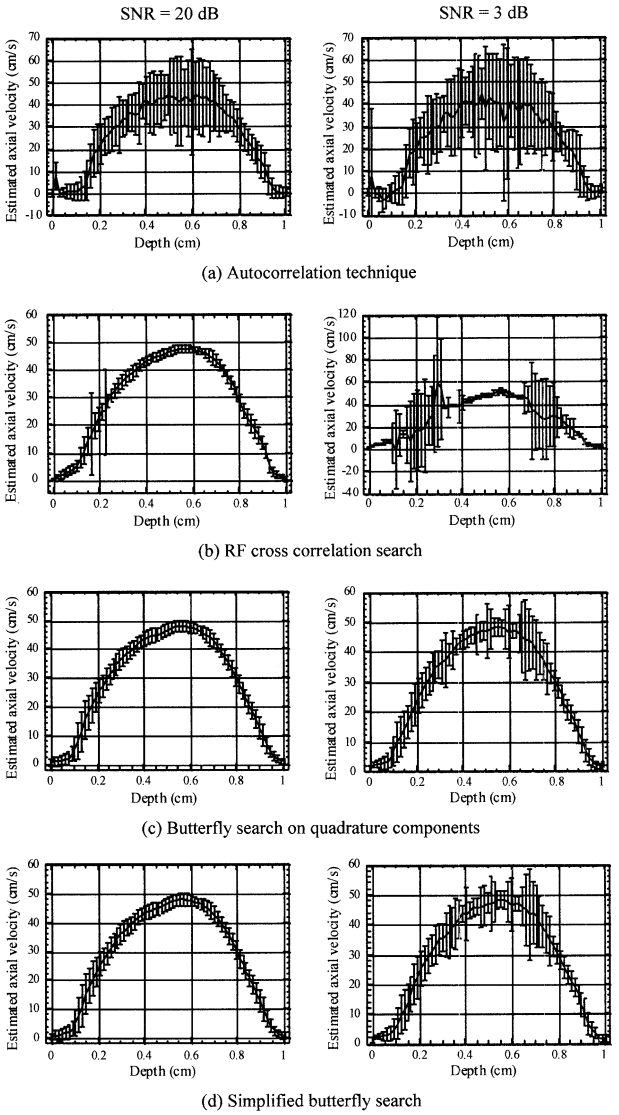

Fig. 8. Mean and SD of different techniques when applied on the Embree M-mode flow phantom data. Number of RF A-lines = 3.

plotted for SNR = 20 dB and SNR = 3 dB in Fig. 8 (number of lines = 3). As expected, we observe that the original butterfly search has the lowest SD, followed closely by the simplified butterfly search at both SNR levels. Notice the different vertical scales for different graphs, especially for RF correlation search at 3 dB. Both the autocorrelation and RF correlation search perform poorly at 3 dB. The autocorrelation method shows large variations even at 20 dB. The cross-correlation technique has large variance close to the wall at 3 dB. We postulate this to be due to higher velocity gradients in the region. M-mode images are created for all the four techniques from these estimated profiles (Fig. 9). The butterfly

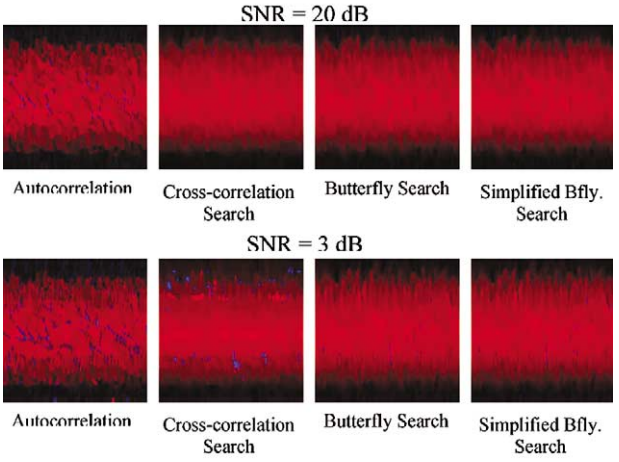

Fig. 9. M-mode images of the estimated velocity profiles using the flow phantom data. Butterfly search clearly outperforms cross-correlation search and autocorrelation. Number of RF A-lines = 3.

search methods show the lowest variation in estimated profile with time (horizontal axis).

DISCUSSION AND CONCLUSION

Various practical issues regarding the implementation of flow imaging are considered in this article. They include frequency-dependent scattering and attenuation, interpolation of $L(\nu)$ peak to reduce computation, use of chirps instead of regular pulses, and wall filtering issues.

The butterfly search technique has been shown to have excellent immunity to noise or other difficult conditions, including decorrelations using simulations and experiments even at a small number of A-lines. McAleavey and Parker (2001) investigated in detail the effect of decorrelation on the performance of the butterfly search. The method's high computational complexity is a limitation. Alam and Parker (1996) discussed two approaches to reduce computational complexity. Additionally, peak interpolation discussed in this article should provide additional reduction. The ability to accurately estimate flow using few A-lines can improve the frame rate of color flow imaging. However, for a given number of A-lines, frame rate is ultimately limited by the PRF due to the range ambiguity problems. In the presence of turbulent flows, since the group of scatterers in the sample volume can break up quickly, estimation is more accurate if it can be performed with few A-lines. At low SNR levels, false peaks in the $L(\nu)$ can sometimes cause large errors. However, due to finite acceleration of blood flow, there would be a temporal correlation between the consecutive estimates (Jensen 1993). Additionally, flow gradients in axial and lateral directions

have to be finite, assuring a spatial continuity of flow in both directions. Thus, in low SNR cases, nonlinear processing techniques like temporal and spatial median filtering may be useful in removing false peaks (Bohs et al. 1993; Jensen 1993). The actual value of the maximum of $L(\nu)$ can shed light on the quality of a given estimate, because it reduces from its possible maximum in nonideal conditions. Turbulence can increase the width of $L(\nu)$ due to the distribution of velocities.

We have observed that increasing the center frequency increases the accuracy of butterfly search techniques (Alam 1996). When longer transmissions are necessary or peak pressure needs to be minimized, chirps can be used instead of pulses to maintain good spatial resolution and low estimation variance. However, frequency-dependent attenuation causes larger attenuation at higher frequencies. It lowers center frequencies with depth. Thus, even when a high-frequency pulse is transmitted, echoes from large depths have lower frequency, nullifying the advantage. Similarly, when chirps are used to increase the band width for longer transmissions, echoes from large depths have higher frequencies attenuated, resulting in lower band width.

We have also discussed wall-filtering issues. Many of the prior art use a single echo-canceller as a wall filter to subtract the successive echoes, and apply flow estimation algorithms on the difference signal. This filter suffers from poor low frequency response. Various complicated wall filters have been proposed to overcome this and other limitations. However, we have demonstrated using simulated data that the butterfly search method can detect flow next to the wall even when blood is highly hypoechoic (clutter 40 dB stronger than blood). The ability of the butterfly search method to detect flow in the presence of strong stationary clutter was particularly evident in the plug flow simulation. Because no wall filtering is applied, bias due to the strong stationary echoes can cause the estimated velocity to be lower than the actual velocity. However, to know only the presence or absence of flow may be sufficient for a diagnosis in many cases. Additionally, a correction that depends on the amplitude of echoes from tissue can possibly be performed; the following approach may be useful. First, $L(\nu)$ is found using the actual data. Then, an average of the A-lines used for the estimation would be substituted for each of the A-lines, and $L(\nu)$ would be found using these lines. This $L(\nu)$ will primarily contain contribution from stationary scatterers and can then be subtracted from the $L(\nu)$ calculated at the beginning to get rid of the effect of the stationary scatterers. We have so far investigated the effect of stationary vessel walls on the velocity estimation using simulated data. Performance of the butterfly search technique in the presence of strong stationary echo needs to be verified *in vivo*. The effect of slowly moving vessel walls also needs to be evaluated. A simple approach may also be useful for the *in vivo* data—just exclude an appropriately chosen range of slow velocities in the $L(\nu)$ search to discard the motion in the slow moving tissues. Wall-filtering is a complex issue and would require additional investigation for a definitive conclusion. Although complete removal of wall-filters may not be advisable, our results point to some interesting possibilities.

VLSI implementation of the butterfly search has been performed (McAleavey 2001). McAleavey also explored one-bit implementation—similar to the one-bit cross-correlation (Bonnefous et al. 1986); one-bit implementation yielded performance similar to that for full-precision signal data when ensemble lengths of eight or greater are used.

Acknowledgement—This work was performed at the University of Rochester and was supported, in part, by the Department of Electrical Engineering and NSF/NYS Center for Electronic Imaging System, University of Rochester, Rochester, NY.

REFERENCES

ATL, Advanced Technology Laboratories. Summary of ATL-sponsored breast ultrasound study and preliminary findings. Bothell, WA: ATL publications, 1994.

Alam SK, Ophir J. The effect of nonlinear signal transformations on bias errors in elastography. IEEE Trans Ultrason Ferroelec Freq Contr 2000;47:297–303.

Alam SK. The butterfly search blood velocity estimation technique for Doppler ultrasound flow imaging. Ph.D. Dissertation, Department of Electrical Engineering, University of Rochester, Rochester, NY, 1996.

Alam SK, Parker KJ. Reduction of computation complexity in the butterfly search technique. IEEE Trans Biomed Eng 1996;43(7): 723–733.

Alam SK, Parker KJ. The butterfly search technique for estimation of blood velocity. Ultrasound Med Biol 1995;21:657–670.

Azimi M, Kak AC. An analytical study of Doppler ultrasound systems. Ultrason Imag 1985;7:1–48.

Bohs LN, Trahey GE. A novel method for angle independent ultrasonic imaging of blood flow and tissue motion. IEEE Trans Biomed Eng 1991;BME-38:280–286.

Bohs LN, Friemel BH, McDermott BA, Trahey E. A real-time system for quantifying and displaying two-dimensional velocities using ultrasound. Ultrasound Med Biol 1993;19:751–761.

Bonnefous O, Pesque P. Time domain formulation of pulse-Doppler ultrasound and blood velocity estimation by cross correlation. Ultrason Imag 1986;8:73–85.

Bonnefous O, Pesque P, Bernard X,. A new velocity estimator for color flow mapping. Proc IEEE Ultrason Symposd 1986:855–860.

Brands PJ, Hoeks APG, Reneman RS. The effect of echo suppression on the mean velocity estimation range of the RF cross-correlation model estimator. Ultrasound Med Biol 1995;21:945–959.

Burns PN. The physical principles of Doppler and spectral analysis. J Clin Ultrasound 1987;15:567–590.

Céspedes I, Huang Y, Ophir J, Spratt S. Methods for estimation of subsample time delays of digitized echo signals. Ultrason Imag 1995;17:142–171.

de Jong PGM, Arts T, Hoeks APG, Reneman RS. Determination of tissue motion velocity by correlation interpolation of pulsed ultrasonic signals. Ultrason Imaging 1990;12:84–98.

Durrani TS, Bisset D. The Radon transform and its properties. Geophysics 1984;49:1180–1187.

Embree PM, Mayo WT. Ultrasonic M-mode RF display technique with application to flow visualization. SPIE Int Symp Pattern Recog Acoust Imaging 1987;768:70–78.

Ferrara KW, Algazi VR. A new wideband spread target maximum likelihood estimator for blood velocity estimation—part I: Theory. IEEE Trans Ultrason Ferroelec Freq Control 1991a;38:1–16.

Ferrara KW, Algazi VR. A new wideband spread target maximum likelihood estimator for blood velocity estimation—Part II: Evaluation of estimators with experimental data. IEEE Trans Ultrason Ferroelec Freq Control 1991b;38:17–26.

Ferrara KW, DeAngelis G. Color flow mapping. Ultrasound Med Biol 1997;23:321–345.

Ferrara KW, Algazi VR, Liu J. The effect of frequency dependent scattering and attenuation on the estimation of blood velocity using ultrasound. IEEE Trans Ultrason Ferroelect Freq Control 1992;39: 754–767.

Foster SG, Embree PM, O'Brien WD Jr. Flow velocity profile via time-domain correlation: Error analysis and computer simulation. IEEE Trans Ultrason Ferroelec Freq Control 1990;37:164–175.

Hein IA, O'Brien WD Jr. Current time-domain methods for assessing tissue motion by analysis from reflected ultrasound echoes—a review. IEEE Trans Ultrason Ferroelec Freq Control 1993b;40:84–102.

Hunt JW, Worthington AE, Kerr AT. The subtleties of ultrasound images of an ensemble of cells: Simulation from regular and more random distribution of scatterers. Ultrasound Med Biol 1995;21: 329–341.

Jensen JA. Detection probabilities for time-domain velocity estimation. Proc. 1991 IEEE Ultrason. Sympos. 1991:1291–1296.

Jensen JA. Range/velocity limitations for time-domain blood velocity estimation. Ultrasound Med Biol 1993;19:741–750.

Jensen JA. Estimation of blood velocities using ultrasound. Cambridge, UK: Cambridge University Press, 1996.

Johnson DH, Dudgeon DE. Array signal processing: Concepts and techniques. Englewood Cliffs, NJ: Prentice Hall, 1993.

Jones SA. Fundamental sources of error and spectral broadening in Doppler ultrasound signals Critical Review. Biomed Eng 1993;21: 399–483.

Kadi AP, Loupas T. On the performance of regression and step-initialized IIR clutter filters for color Doppler systems in diagnostic medical ultrasound. IEEE Trans Ultrason Ferroelec Freq Control 1995;42:927–937.

Kasai C, Namekawa K, Koyano A, Omoto R. Real-time two-dimensional blood flow imaging using an autocorrelation technique. IEEE Trans Sonics Ultrason 1985;32:458–464.

Kremkau FW. Doppler ultrasound: Principles and instruments. Philadelphia, PA: Saunders, 1990.

Kremkau FW. Principles of color flow imaging. J Vasc Tech 1991;15: 104–111.

Loupas T, Gill RW. Multi-frequency Doppler. Improving the quality of spectral estimation by making full use of the information present in the backscattered RF echoes. IEEE Trans Ultrason Ferroelec Freq Control 1994;41:522–531.

Loupas T, Powers JT, Gill RW. An axial velocity estimator for ultrasound blood flow imaging, based on a full evaluation of the Doppler equation by means of a two-dimensional autocorrelation approach. IEEE Trans Ultrason Ferroelect Freq Control 1995;42:672–688.

Magnin PA. Doppler effect: History and theory. Hewlett-Packard J 1986;37:26–31.

Magnin PA. A review of Doppler flow mapping techniques. Proc. 1987 IEEE Ultrason. Sympos. 1987:969–977.

McAleavey S. Implementation issues for butterfly search velocity estimation. Ph.D. Dissertation. Department of Electrical Engineering, University of Rochester, Rochester, NY, 2001.

McAleavey S, Parker KJ. Effect of decorrelation on butterfly search velocity estimator performance. In: Shung KK, Insana MF, eds. Medical imaging 2001: Ultrasonic imaging and signal processing. Proceedings of SPIE. Vol. 4325. Bellingham, WA: SPIE 2001:293–304.

Nowicki A, Reid J, Pedersen PC, Schmidt AW, Oung H. On the behavior of instantaneous frequency estimators implemented on Doppler flow imagers. Ultrasound Med Biol 1990;16:511–518.

Peterson RB, Atlas LE, Beach KW. A comparison of IIR initialization techniques for improved color Doppler wall filter performance. Proc. 1995 IEEE Ultrason. Sympos. 1995:1705–1708.

Rajaonah JC, Dousse B, Meister JJ. Compensation of the bias caused by the wall filter on the mean Doppler frequency. IEEE Trans Ultrason Ferroelec Freq Control 1994;41:812–819.

Rao NAH, Ritenour ER, Hendrick RE. Frequency modulated pulse for ultrasonic imaging. Proc SPIE Med Imag.-II 1988;914:67–74.

Rickey DW, Rankin R, Fenster A. A velocity evaluation phantom for color and pulsed Doppler instruments. Ultrasound Med Biol 1992; 18:479–494.

Shariati MA, Dripps JH, McDicken WN. Deadbeat IIR based MTI filtering for color flow imaging systems. Proc. 1993 IEEE Ultrason. Sympos. 1993:1059–1063.

Suorsa V, Kerr AT, Hunt JW, O'Brien WD Jr. Influence of stationary signals on the time-domain correlation blood flow measurement. Proc. 1990 IEEE Ultrason. Sympos. 1990:1563–1566.

Thomas L, Hall A. An improved wall filter for flow imaging of low velocity flow. Proc. 1993 IEEE Ultrason. Sympos. 1993:1701–1704.

Torp H, Kristoffersen K. Velocity matched spectrum analysis: A new method for suppressing velocity ambiguity in pulsed-wave Doppler. Ultrasound Med Biol 1995;21:937–944.

Tysoe C, Evans DH. Bias in mean frequency estimation of Doppler signals due to wall clutter filters. Ultrasound Med Biol 1995;21: 671–677.

Vaitkus PJ. A new time-domain narrowband velocity estimation technique for Doppler ultrasound flow imaging, Ph.D. dissertation, Dept Elect Comput Eng., Univ. Toronto, 1995.

Vaitkus PJ, Cobbold RSC. A new time-domain narrowband velocity estimation technique for Doppler ultrasound flow imaging. IEEE Trans Ultrason Ferroelec Freq Control 1998;45(4):939–954.

Vogt M, Ermert H. Application of high frequency broadband ultrasound for high resolution blood flow measurement. Proc. 1997 IEEE Ultrason. Sympos. 1997:1243–1246.

Wells PNT. Ultrasonic color flow imaging. Phys Med Biol 1994;39: 2113–2145.

Wending F, Jones SA, Giddens DP. Simulation of Doppler ultrasound signal for a laminar, pulsatile, nonuniform flow. Ultrasound Med Biol 1992;18:179–193.

Willemetz JC, Nowicki A, Meister JJ, de Palma F, Pante G. Bias and variance in the estimate of the Doppler frequency induced by a wall motion filter. Ultrason Imaging 1989;11:215–225.

Wilson LS. Description of broad-band pulsed Doppler ultrasound processing using the two-dimensional Fourier transform. Ultrason Imaging 1991;13:301–315.